Signatures of nanoemulsion jamming and unjamming in stimulated-echo NMR

Yixuan Xu [1,*] Madison L. Nelson [2,*] Joseph D. Seymour [3,†] and Thomas G. Mason [4,5,‡]

[1]*Department of Materials Science and Engineering, University of California–Los Angeles, Los Angeles, California 90095, USA*
[2]*Department of Physics, Montana State University, Bozeman, Montana 59717-3920, USA*
[3]*Department of Chemical and Biological Engineering, Montana State University, Bozeman, Montana 59717-3920, USA*
[4]*Department of Chemistry and Biochemistry, University of California–Los Angeles, Los Angeles, California 90095, USA*
[5]*Department of Physics and Astronomy, University of California–Los Angeles, Los Angeles, California 90095, USA*

(Received 15 September 2022; accepted 20 January 2023; published 9 February 2023)

The unjamming of elastic concentrated nanoemulsions into viscous dilute nanoemulsions, through dilution with the continuous phase, offers interesting opportunities for a pulsed-field gradient (PFG) NMR, particularly if the nanoemulsion is designed to take advantage of the nuclear specificity offered by NMR. Here, we make and study size-fractionated oil-in-water nanoemulsions using a perfluorinated copolymer silicone oil that is highly insoluble in the aqueous continuous phase. By studying these nanoemulsions using ^{19}F stimulated-echo PFG-NMR, we avoid any contribution from the aqueous continuous phase, which contains a nonfluorinated ionic surfactant. We find a dramatic change in the ^{19}F PFG-NMR decays at high field-gradient strengths as the droplet volume fraction, ϕ, is lowered through dilution. At high ϕ, observed decays as a function of field-gradient strength exhibit decay-to-plateau behavior indicating the jamming of nanodroplets, which contain ^{19}F probe molecules, in an elastic material reminiscent of a nanoporous solid. In contrast, at lower ϕ, only a simple decay is observed, indicating that the nanodroplets have unjammed and can diffuse over much larger distances. Through a comparison with bulk mechanical rheometry, we show that this dramatic change coincides with the loss of low-frequency shear elasticity of the nanoemulsion.

DOI: 10.1103/PhysRevE.107.024605

I. INTRODUCTION

Nuclear magnetic resonance (NMR) is a powerful and sensitive experimental technique that can reveal structure and dynamics within both simple homogeneous and complex heterogeneous forms of condensed matter. Pulsed-field gradient (PFG) NMR provides access to the dynamics of molecules which contain specific nuclei of interest [1]. In one particular application of PFG-NMR, investigations of the dynamics of liquid molecules in nanoporous solids have revealed the very substantial impact of molecular confinement within nanopores [2]. Because the nanopores are sufficiently small, the high degree of spatial confinement of the liquid molecules, as these experience quiescent Brownian excitations, can be readily detected at high field-gradient strengths. Instead of exhibiting a simple exponential decay, as in a bulk liquid, the PFG-NMR signal does not fully decay when a liquid is so highly confined within nanopores. The substantial impact of nanoporous confinement on molecular diffusion has been observed using ^{1}H PFG-NMR and reported for polydimethylsiloxane silicone oil in open-pore polymeric host matrices [3], water in single-walled carbon nanotubes [4], hexadecane in core-shell latex particles [5], hexane in nanoporous zeolite crystallites [6], and eicosane in electrochemically etched silicon nanochannels [7]. In particular, the simple exponential decay associated with molecular diffusion in the bulk liquid can transition to a decay-to-plateau behavior [8] for the same liquid that is highly confined within a nanoporous solid [2].

Investigating the molecular dynamics of polymers subjected to shear or flow has opened up an application of PFG-NMR equipped with rheometer components, known as Rheo-NMR [9,10]. Probe molecules can either be attractively bound to or repulsively confined by other neighboring molecules; examples include a solid phase of bulk polymers [9,11] and a glassy state of concentrated polymer solutions [12]. Different techniques, such as NMR spectroscopy, relaxometry, diffusivity, and velocity imaging, have been applied to study the microscopic response to shear- and flow-induced anisotropy in bulk materials [11–14]. While these prior Rheo-NMR experiments have combined certain aspects of rheology and NMR, so far these approaches have not been based on the notions of passive microrheology [15], even as such a possibility has been suggested previously [16].

Nanoemulsions are dispersions of liquid droplets having sub-100 nm radii in an immiscible continuous solution phase that are stabilized against subsequent coalescence by a surfactant [17–19]. Customized nanoemulsions are continuously being developed and applied in many different areas, including pharmaceuticals and industrial products [20]. Although the nanoemulsion is composed entirely of liquids, if the volume fraction of droplets, ϕ, is raised beyond the jamming point, a well-stabilized nanoemulsion becomes a soft elastic solid as a consequence of a combination of interfacial

*These authors contributed equally to this work.
†jseymour@montana.edu
‡mason@chem.ucla.edu

tension and interfacial repulsion between the jammed nanodroplets in close proximity [21]. These jammed nanodroplets are confined by neighboring nanodroplets, and the positional structure of the solid nanoemulsion resembles that of a disordered glass in the absence of strong interdroplet attractions [19]. Concentrated nanoemulsions can mimic disordered closed-pore nanoporous solids when ϕ is above the jamming point. Interestingly, this nanoporous solid can effectively be melted through dilution with sufficient continuous-phase solution, thereby lowering ϕ below the jamming point. Thus, nanoemulsions could provide a route for studying what happens to molecular dynamics when an elastic closed-pore nanoporous material is melted as the pores (i.e., nanodroplets) effectively transition from being confined to unconfined as ϕ is reduced. If the nanoemulsion could be customized appropriately, in principle, PFG-NMR could then be used to probe the dynamics of only the dispersed-phase oil molecules within the nanodroplets, and thus could potentially provide a sensitive means of exploring droplet unjamming as the closed-pore nanoporous solid melts, since the molecular dynamics are inherently coupled to the nanodroplets' dynamics.

While ^{1}H PFG-NMR has many different important uses, its potential application for studying confined molecular diffusion in simple oil-in-water nanoemulsions would likely be difficult to interpret because hydrogen is extensively present both in the water of the continuous phase as well as in the most common hydrocarbon and silicone oils in the dispersed droplet phase [22]. Consequently, it would be desirable to consider ^{19}F PFG-NMR as an alternative, since this can create comparably strong signals as ^{1}H PFG-NMR. Silicone oils having perfluorinated side groups offer a potential route for developing a stable oil-in-water nanoemulsion, in which ^{19}F-laden silicone oil molecules are present only within the interior of the constituent nanodroplets. While prior experiments demonstrated that stable perfluorinated silicone oil-in-water nanoemulsions could be produced, these experiments relied upon a perfluorinated surfactant soluble only in the aqueous continuous phase [23]. Such use of a perfluorinated surfactant in combination with a perfluorinated oil would be less desirable, since ^{19}F PFG-NMR would yield a convolution of signals from surfactant molecules experiencing unconfined diffusion in the continuous phase, adsorbed surfactant molecules diffusing on the interfaces of nanodroplets, and also oil molecules experiencing confined diffusion within the nanodroplets.

Consequently, in order to study only the dynamics of the oil molecules within nanodroplets, it would be desirable to formulate a special customized perfluorinated oil-in-water nanoemulsion that is extremely stable even when concentrated to high ϕ above jamming, yet does not rely upon perfluorinated surfactant for stability. In addition, it would be desirable for this nanoemulsion to have a narrow droplet size distribution, and also for the perfluorinated silicone oil to be very highly insoluble in the aqueous continuous phase so that interdiffusion of oil molecules between different nanodroplets, which can lead to Ostwald ripening, is avoided. For such a highly customized nanoemulsion, in principle, the total average molecular motion of ^{19}F-laden oil molecules would depend in part on the degree of nanodroplet motion and hence ϕ relative to the nanodroplet jamming point. Detecting nanodroplet unjamming by reducing ϕ in such a customized perfluorinated nanoemulsion would be an important first step towards finding a way to use PFG-NMR for quantitative passive microrheology based on inferred motion of colloidal structures (i.e., nanodroplets), as has been previously suggested more broadly.

This overall approach is different from prior investigations involving PFG-NMR on other emulsion systems. Several of these investigations have focused on extracting distributions of droplet (i.e., cavity) sizes by fitting the signal attenuation, typically assuming a log-normal distribution [24–27]. Moreover, for emulsions in which the dispersed phase has a reasonably high solubility in the continuous phase, complex transport of molecules can be observed as these molecules hop intermittently from one droplet to another through the continuous phase [28,29], akin to transport of liquid molecules in solid open-pore porous media having larger cavities and narrow constrictions [30]. While some PFG-NMR studies of emulsions have been made previously, examining how droplet jamming and unjamming in highly concentrated monodisperse nanoemulsions affects PFG-NMR attenuation still remains largely unexplored.

Here, we have created a customized, size-fractionated, highly stable ^{19}F-oil-in-water nanoemulsion system, having screened-charge repulsive droplet interactions, that provides a useful model system, and we show using ^{19}F StE PFG-NMR that droplet jamming can lead to a strong subdiffusive signal in the effective molecular-probe MSDs. We obtain high-quality functional fits of the effective MSDs, showing a smooth rise-to-plateau transition at each higher ϕ above the droplet jamming point. Through a comparison with macroscopic rheological measurements, we associate the changes in these effective MSDs with the rheological transition between viscous unjammed nanoemulsions at lower ϕ and elastic jammed nanoemulsions at higher ϕ. Furthermore, by interpreting the mechanical measurements using the theoretical framework of passive microrheology, we extract plateau MSDs of nanodroplets in elastic nanoemulsions at high ϕ. By combining both NMR measurements with the passive microrheological interpretation of these mechanical measurements, we show that the nanoemulsion's unjamming transition is consistent with a Lindemann melting criterion of 0.3 known for a wide range of materials [31].

II. EXPERIMENT

A. Emulsion preparation and characterization

We have designed and prepared an oil-in-water fluorinated nanoemulsion (O/W FNEM) composed of 48%:52% poly-(3,3,3-trifluoropropyl-methylsiloxane):poly-(dimethylsiloxane) block copolymer (FMS oil, Gelest Inc.; mass density: $\rho_o = 1.16$ g mL^{-1}; average molecular weight: $MW_o = 1800$ g mol^{-1}; kinematic viscosity: $\nu_o = 124$ cSt), sodium dodecyl sulfate (SDS, Fisher Scientific; electrophoresis grade 99% purity), and deionized water (Millipore Milli-Q Academic; resistivity: 18.2 MΩ cm). After conducting a series of emulsification and stability screening tests using a variety of ^{19}F-containing oils, we have selected block-copolymer FMS because it is highly perfluorinated

to provide strong NMR signal-to-noise, it has a low enough viscosity to facilitate fabrication of a nanoemulsion using only high flow-rate emulsification processing without evaporative ripening [18,19,32], it has a high enough molecular weight to preclude Ostwald ripening, and it remains stable against coalescence when using only a standard nonperfluorinated ionic surfactant, SDS. Because FMS is highly insoluble in the continuous aqueous phase, as revealed by the absence of Ostwald ripening, the ^{19}F-laden oil molecules do not migrate appreciably through the continuous phase from one droplet to another. Also, our use of a nonfluorinated SDS surfactant, which is atypical in most formulations of stable fluorinated O/W emulsions, ensures that all NMR signals arise from the fluorinated oil inside nanoemulsion droplets without any contribution from the surfactant.

We initially prepare 500 mL of a crude microscale premix emulsion at a droplet volume fraction $\phi = 0.15$ of FMS oil in 50 mM aqueous SDS solution using a mixer (Fisher Scientific, PowerGen 1000 S1, speed 3). After allowing any residual foam to disappear, we process this premix emulsion using a high flow rate microfluidic homogenizer (Microfluidics Inc., model M-110P; 75 μm Y-chamber) at a liquid pressure of approximately 200 MPa. We recover and reprocess the resulting nanoemulsion through this homogenizer seven additional times before collecting and diluting the resulting nanoemulsion in 10 mM aqueous SDS solution. We centrifuge this diluted nanoemulsion to obtain a much higher droplet volume fraction (Beckman L8-55 ultracentrifuge, SW-28 swinging bucket, 18 000 rpm, 4 h), yielding a set of concentrated, elastic, jammed nanoemulsion plugs at the bottoms of thick-wall polycarbonate centrifuge tubes. The effective gravitational forces acting on droplets, caused by this ultracentrifugation, are still small enough that nanodroplet coalescence is not observed. We next remove the SDS solution above these elastic concentrated nanoemulsion plugs, combine these plugs together, and then dilute these combined plugs to $\phi \approx 0.1$ using an aqueous solution at [SDS] = 10 mM. This process of centrifugation and dilution is repeated twice more to set the SDS concentration in the continuous phase of the resulting FNEM to 10 mM.

To decrease the droplet size polydispersity of this FNEM, we perform a four-step size-fractionation at fixed [SDS] = 10 mM as follows. After a first centrifugation for size-fractionation (conditions also 18 000 rpm, 4 h), we remove the concentrated elastic nanoemulsion plugs from the bottoms of the centrifuge tubes, cut them into two pieces using a spatula, and retain the bottom three-quarters of all plugs, corresponding to larger droplets. We combine and dilute these bottom plug-pieces using 10 mM SDS solution to set $\phi \approx 0.1$. We then perform a second centrifugation using the same conditions, cut the plugs, retain and combine the top three-quarters of the plugs, and again dilute using 10 mM SDS solution to set $\phi \approx 0.1$. We then perform a third centrifugation using the same conditions and procedure as above, and the top half of the plugs are combined and diluted to $\phi \approx 0.1$ in 10 mM SDS solution. Finally, we perform a fourth centrifugation using the same conditions and procedure, and we retain and combine the bottom three-quarters of the plugs, yielding ≈20 g of concentrated, fractionated master nanoemulsion, which is a soft elastic solid, at high ϕ. We next mix this master nanoemulsion thoroughly using a spatula to exclude any size-separation that could potentially be induced by centrifugation. The oil droplet volume fraction of the master nanoemulsion sample is measured to be $\phi_m = 0.751 \pm 0.008$ using a gravimetric evaporation method [33]. Using dynamic light scattering (Photocor, 90° scattering angle, $\lambda = 632.8$ nm), the average droplet radius of this fractionated FNEM is measured to be $\langle a \rangle = 63 \pm 2$ nm, and its radial size polydispersity is $\delta a/\langle a \rangle = 0.16$, where δa is the standard deviation of the emulsion's radial size distribution. FNEM samples at lower ϕ are obtained by diluting a portion of the master nanoemulsion with an aqueous 10 mM SDS solution using an analytical balance (Denver Instruments APX-200, 0.1 mg precision). Based on prior experiments on similarly fabricated, stabilized, and fractionated O/W nanoemulsions, the droplet structure in the fractionated O/W FNEMs is disordered at all the ϕ we explore. Moreover, the pair interaction between two FNEM nanodroplets can be described by a screened electrostatic repulsion having a Debye screening length $\lambda_D \approx 3$ nm.

Each FNEM sample is loaded into a clean glass NMR tube, having an inner diameter of 8 mm, to a height of at least 25 mm from the bottom of the tube, as follows. For $0.248 \leqslant \phi \leqslant 0.420$, we load these viscous FNEM samples by pouring against the walls of tubes very slowly in order to avoid creating any air bubbles. For soft elastic FNEM samples at higher $0.480 \leqslant \phi \leqslant 0.751$, we load each into a NMR tube with a spatula and perform a low-speed centrifugation for a short duration to remove air bubbles without generating gradients in ϕ. The maximum centrifugal speed does not exceed 1500 rpm. The total duration, including acceleration and deceleration, varies from 60 to 1200 s; this duration is increased to 1200 s as ϕ is raised toward 0.751. After loading, we cap the NMR tubes with plastic caps and apply Parafilm to seal them, thereby precluding evaporation, which could otherwise lead to undesirable changes in ϕ and ultimately droplet coalescence.

B. Stimulated-echo ^{19}F-NMR

The samples in 8 mm glass NMR tubes are stored upright at room temperature until measurements. We perform all diffusion measurements using a Bruker 250 MHz superconducting magnet with a Micro5 probe base and 8 mm rf coil (Bruker Biospin, Karlsruhe) for ^{19}F nuclei excitation and detection, integrated with a Diff30 gradient coil providing 17.81 T/m pulsed magnetic field gradients at 60 A in the z-direction of the applied magnetic field. We hold the temperature stable at 20 °C through the Bruker BTU system with N_2 gas flow and active feedback control. For the diffusion measurements, we utilize a standard pulsed-field gradient stimulated echo (PFG-StE) pulse sequence [27]. In these experiments, we implement a constant gradient duration δ and diffusion displacement time Δ between gradient pulses and increasing gradient strength g to step through the displacement reciprocal wavelength $q = (2\pi)^{-1}\gamma\delta g$ space, where γ is the gyromagnetic ratio of the ^{19}F nuclei. This standard implementation of the PFG-StE sequence allows the mean-square displacement (MSD) to be calculated from the normalized echo voltage signal as $E(q) = S(q)/S(q=0) = \exp[-4\pi^2 q^2(\Delta - \delta/3)] = \exp(-2\pi^2 q^2 \langle z^2 \rangle)$, where $\langle z^2 \rangle = 2D(\Delta - \delta/3)$ is the one-dimensional (1D) MSD, and D is the molecular diffusion

coefficient [27]. This equation is also often written in terms of the effective diffusion using the nomenclature $E(b) = S(b)/S(b=0) = \exp(-bD_{\text{eff}})$, where an effective gradient and displacement time parameter $b = 4\pi^2 q^2(\Delta - \delta/3) = (\gamma\delta g)^2(\Delta - \delta/3)$ is used to reflect the displacement time dependence inherent in D_{eff} [27].

Additionally, we vary the gradient duration δ and displacement time Δ to optimize the measurements for probing the MSD of the nanoemulsion droplets. The molecular diffusion coefficient of the FMS oil is measured to be 4.19×10^{-12} m^2/s. The value of $\Delta = 700$ ms ($\gg \langle a\rangle^2/D_0 = 9.47 \times 10^{-3}$ ms) provides the long-time asymptotic MSD of the droplets by allowing the fluorinated polymer to fully sample the interior of the nanoemulsion droplets and the droplets to diffuse within the emulsion structure [28,34]. To provide additional data on the emulsion structure in terms of a porous media, we examine a range of δ values from 2 to 5 ms, for which $\delta \gg \langle a\rangle^2/D_0$, to observe the signal dependence on the varying gradient durations [28,30,34]. For all experiments reported here, we use a gradient duration $\delta = 2$ ms, which for the particle motion scale results in $l_{\text{D}} = \sqrt{2D_{\text{SE}}\delta} = 1.67 \times 10^{-7}$ m, equivalent to $1.85\langle a\rangle$, which generates a small additional signal attenuation in the dilute system, accounted for by the $\delta/3$ in the definition of b, which results in no relaxation weighting of the diffusion data based on the measurement of a single T_2 relaxation time of 291 ms observed using a Carr-Purcell Meiboom-Gill [35] experiment. We report measurements over a wide range of ϕ from 0.751 down to 0.1. Having a single relaxation time larger than the δ indicates the signal does not decay significantly during the gradient duration, corresponding to no relaxation weighting of the diffusion data. We increment gradients from 0.89 up to 17.81 T/m with 32 linearly spaced steps. For each gradient step, we perform ensemble averaging of a 16-step phase cycle eight times.

C. Mechanical shear rheometry

We first ensure proper calibration of our strain-controlled shear rheometer (Rheometrics RFS-II), both in the magnitude of the complex shear modulus and crossover frequency, using a polymeric viscoelastic reference standard. Following calibration, for samples having $0.359 \leqslant \phi \leqslant 0.751$, we load each FNEM into a 25-mm-diameter stainless-steel cone-and-plate geometry enclosed by a vapor trap. At a shear strain $\gamma = 0.01$, we perform a frequency sweep from frequency $\omega = 10$ rad/s down to 0.02 rad/s. We then perform a strain sweep at $\omega = 1$ rad/s from $\gamma = 0.002$ to 2 to verify that the strain of 0.01 selected for the frequency sweep is below the yield strain, ensuring that reported G'_{p} values for $0.373 \leqslant \phi \leqslant 0.751$ correspond to the linear stress-strain response regime. For $\phi = 0.365$, the low-strain storage shear modulus $G'(\gamma)$ is effectively identical to the loss shear modulus $G''(\gamma)$ at $\gamma \leqslant 0.02$. For more highly diluted samples having $\phi \leqslant 0.360$, $G''(\gamma)$ dominates $G'(\gamma)$ even at small shear strains. We determine the dynamic viscosity of the FMS bulk oil, using steady shear rate sweep measurements, to be $\eta_{\text{o}} = 143$ mPa s. The measured shear stress τ varies linearly with the shear strain rate $\dot{\gamma}$ from 1000 to 0.2 s^{-1}. Using the mass density of the FMS oil, we then convert to the kinematic viscosity: $\nu_{\text{o}} = 124$ cSt.

III. RESULTS

A. NMR magnetization decay and MSD analysis

Using a fitting procedure, we normalize the StE PFG-NMR magnetization attenuation, $E(b) = S(b)/S(b=0)$, determined by varying g at fixed $\Delta = 700$ ms, so that it decays exponentially from unity in the low-b (i.e., low-q^2) limit. This ensures that dimensionless $-\ln[E(b)]$, which is proportional to the ensemble- and time-average MSD of the probes, rises linearly with b in a double-logarithmic scale at low b for all ϕ [open circles in Fig. 1(a)]. For all ϕ, we have also subtracted the small baseline noise signal of $E(b)$ before normalizing; this baseline is determined by the measured noise plateau in $E(b)$ beyond the decay at high b only at low ϕ where the samples are purely viscous and simple diffusion of ^{19}F-laden FMS oil molecules is observed. This baseline noise subtraction makes no more than a 5% adjustment in the values of $E(b)$ over all ϕ measured.

We fit the measured dimensionless MSDs to a simple diffusion model for lower ϕ and to a bound diffusion model (called the single exponential model in Magin *et al.* [8]) for higher ϕ:

$$-\ln[E(b)] = \begin{cases} bD_0, & \phi \leqslant \phi_{\text{c}}, \\ (D_0/D_1)[1 - \exp(-bD_1)], & \phi > \phi_{\text{c}}, \end{cases} \quad (1)$$

where D_0 is the low-b diffusion coefficient, ϕ_{c} is a critical nanodroplet volume fraction associated with droplet jamming and the onset of subdiffusive behavior in the decay at high b, and D_0/D_1 indicates the relative amount of decay, corresponding to the plateau of the MSD in the high-b limit [solid lines in Fig. 1(a)]. This high-b plateau is also reminiscent of harmonically bound Brownian behavior [36]. From our measurements, recognizing that the limited upper range of b of our measurement window could have some impact on the exact value, we find $\phi_{\text{c}} \approx 0.32$ is an empirical volume fraction threshold below which the attenuation signal can be described as a simple exponential decay corresponding to a diffusive random walk. Using the determined fit parameters, we also plot the normalized $E(b)$ data with lines that correspond to the exponential of Eq. (1):

$$E(b) = \begin{cases} \exp(-bD_0), & \phi \leqslant \phi_{\text{c}}, \\ \exp\{-(D_0/D_1)[1 - \exp(-bD_1)]\}, & \phi > \phi_{\text{c}}, \end{cases} \quad (2)$$

as shown in Fig. 1(b). The trend toward nonzero positive values of a plateau in $E(b)$ at high b is clearly seen; this is associated with subdiffusive measured log-slopes of $-\ln[E(b)]$ at high b.

Nanodroplet unjamming behavior, as ϕ is reduced and the FNEM transitions rheologically from elastic solid to a viscous liquid, is clearly seen through the large changes in the observed NMR $E(b)$. To understand and describe this, we assume that the total MSD of ^{19}F-probe-molecules arises from a combination of confined internal molecular diffusion of the FMS oil within nanodroplets and also the diffusion of nanodroplets in the aqueous continuous phase—yet modified by interactions with neighboring nanodroplets that can lead to nanodroplet confinement through jamming at high ϕ. The viscosity of the bulk fluorinated oil is 143 mPa s, determined by mechanical shear rheometry. The NMR measurements determine the translational diffusion coefficient of the bulk oil to be 4.19×10^{-12} m^2 s^{-1}, yielding a viscosity of

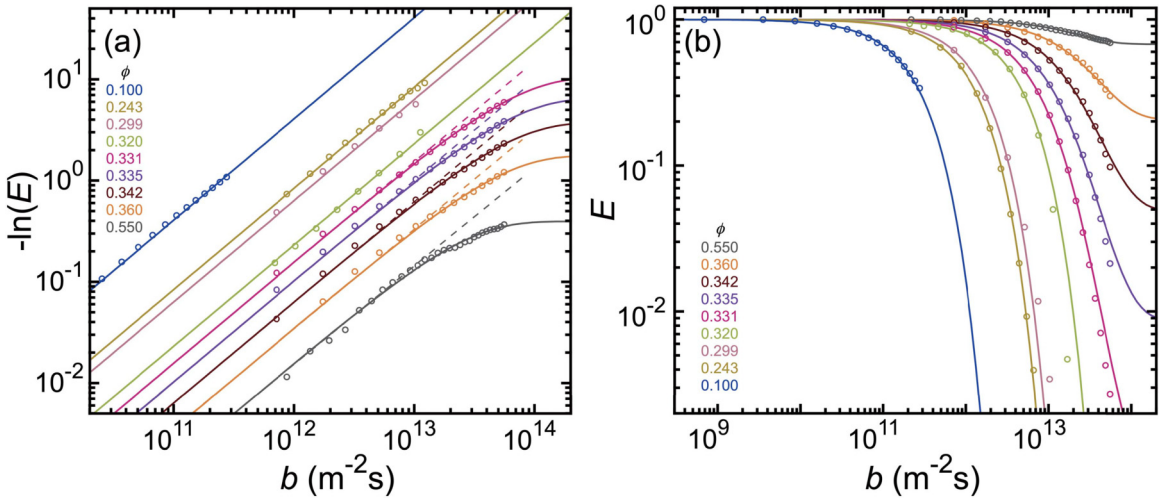

FIG. 1. (a) Effective mean-square displacements (MSDs) of the ^{19}F-laden oil molecules of the O/W nanoemulsions having an average droplet radius $a = 63$ nm for a different droplet volume fraction ϕ (color-encoded, see left), represented by the negative natural logarithm of the corrected StE PFG-NMR diffusion signal attenuation, $-\ln[E(b)]$, measured at diffusion time between refocused pulses $\Delta = 700$ ms and gradient pulse duration $\delta = 2$ ms. Solid lines are functional fits to Eq. (1). For $\phi \geqslant 0.331$, the departure from low-b diffusive $-\ln[E(b)]$ behavior (dashed lines show the extension toward high-b) occurs at $b \approx 5 \times 10^{12}$ m^{-2} s. The largest b at the maximum experimentally explored gradient strength is $b_{\max} = 5.6 \times 10^{13}$ m^{-2} s. (b) Effective correlation functions of the FNEM, represented by baseline-subtracted and normalized attenuation, $E(b)$. The lines represent calculations using Eq. (2) and parameters from the corresponding functional fits in part (a). The order of ϕ goes from top to bottom in the caption of part (a) and from left to right in part (b).

128 mPa s according to the Stokes-Einstein relation, using the macromolecular radius of gyration of 0.4 nm. The difference between these two measurements is within 11%. The diffusion time between two adjacent refocused pulses and the duration of gradient pulses are fixed at $\Delta = 700$ ms and $\delta = 2$ ms, respectively, in all reported NMR measurements. For a higher ϕ above the unjamming, the NMR magnetization decays at a lower rate and exhibits less attenuation at high b, reflecting the confinement from droplet jamming [Fig. 1(b)]. The decay signal in the high-ϕ regime can be fit to the bound diffusion model, showing a concave-up bending towards a plateau as b increases [Eq. (2) for $\phi > \phi_c$]. In the high-ϕ regime, the droplet motion is geometrically restricted in the cage formed by adjacent droplets so that droplet diffusion contributes less in the combined apparent probe diffusion. When the emulsion is diluted to lower ϕ, a viscous response is obtained and the magnetization attenuation can be fit to a single exponential model [Fig. 1(b) and Eq. (2) for low $\phi \leqslant \phi_c$]. In the low-ϕ regime, the mobility of a droplet in the emulsion, having a high-frequency viscosity close to water's 1 mPa s, is much higher with respect to the mobility of a confined ^{19}F probe molecule in the droplet whose viscosity is more than a hundredfold higher. Therefore, the droplet diffusion predominates the confined probe molecular diffusion and effectively results in the apparent diffusive behavior of the probe that can be detected by NMR.

The transition in NMR magnetization decay features above and below the droplet unjamming can be more readily seen in the $-\ln E(b)$ functions, where $-\ln E$ is proportional to the mean-square displacements of the probe [Eq. (2) and Fig. 1(a)]. Linear correlation between $-\ln E$ and b over the entire explored b range is observed for an unjammed emulsion having low $\phi \leqslant 0.320$. By contrast, dense emulsions having high $\phi \geqslant 0.325$ present a linear rise at low b, followed by a bending knee as b is varied from low to high. Independent of ϕ, the divergence from the linearity occurs at $b \approx 5 \times 10^{12}$ m^{-2} s.

The influence of droplet confinement on NMR magnetization decay is revealed distinctly in the $-\ln E(b)$ log-slope plot as a function of ϕ [Fig. 2(a)]. At a given ϕ, the log-slope (i.e., the MSD scaling exponent, represented by the slope of the log-log plot of the effective MSD [37]) is calculated from the first derivative of the fitting function Eq. (1) and evaluated at the maximum measured $b_{\max}$. A gradual increase in the $b_{\max}$-log-slope is observed from high ϕ down to $\phi \approx 0.34$, followed by an abrupt increase until ϕ approaches 0.32; and by definition, the log-slope is strictly equal to unity for $\phi \leqslant 0.32$. The ratio of D_0/D_1, obtained from the fits using Eq. (1) for $\phi > \phi_c$, is associated with the amount of magnetization decay observed at high b. As ϕ is decreased, D_0/D_1 increases slowly in the high-ϕ regime, bends up more rapidly near $\phi \approx 0.4$, and diverges at $\phi \approx 0.33$ [Fig. 2(b)]. The diffusion coefficient D_0, representing the low-b diffusibility, is fit to a four-parameter function having a cubic decrease multiplied by a Fermi-like function [see the caption to Fig. 2(c)]. In the high-ϕ regime where droplets are jammed, the droplet is highly confined by the cage of its nearest-neighboring droplets, and the internal double-bound molecular probe exhibits low diffusibility, reflected by the low magnitude of $D_0 \approx 2 \times 10^{-14}$ m^2 s^{-1} for $\phi \geqslant 0.38$. As ϕ is reduced, a rapid exponential rise of D_0 is observed, attributed to a weaker cage effect, reflecting the droplet unjamming in the range $0.38 \geqslant \phi \geqslant 0.30$. As further diluted to lower ϕ, the measured D_0 gradually increases towards the diffusion coefficient of an isolated droplet in water near 3.4×10^{-12} m^2 s^{-1}, calculated by the Stokes-Einstein relation, which declares that the droplet diffusion confinement disappears. The uncertainty of the fitting parameter $D_{0,d} \approx 5.5 \times 10^{-12}$ m^2 s^{-1} is comparable to its value due to

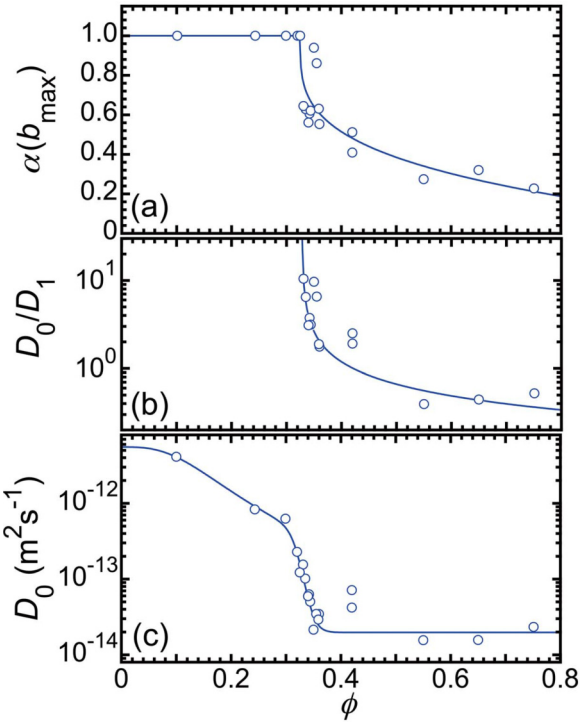

FIG. 2. High-b log-slope and fitting parameters of the effective MSDs, $-\ln[E(b)]$, as functions of ϕ. (a) Log-slope of $-\ln[E(b)]$ approaching the maximum measured b, $\alpha(b_{\max}) = d\ln[-\ln(E)]/d\ln(b)$ evaluated at $b_{\max}$, calculated from the $-\ln[E(b)]$ fits [solid lines in Fig. 1(a)] and fit to 1 for $\phi \leqslant \phi_c$; and $1-(\phi-\phi_c)^n$ for $\phi > \phi_c$, where $\phi_c = 0.325 \pm 0.011$, and $n = 0.28 \pm 0.04$ (square of the correlation coefficient: $R^2 = 0.835$). (b) The ratio D_0/D_1, representing the amount of attenuation at high-b, obtained from fits using Eq. (1) for each given $\phi \geqslant 0.325$ and fit to $D_0/D_1(\phi) = [\phi_m/(\phi-\phi_c)]^\nu$, where $\phi_c = 0.328 \pm 0.007$, $\phi_m = 0.09 \pm 0.05$, and $\nu = 0.67 \pm 0.30$ ($R^2 = 0.751$). (c) The low-b diffusion coefficient D_0 for all measured ϕ obtained from Eq. (1) and fit to $D_0(\phi) = \{D_{0,d}/[1+(\phi/\phi_v)^3]\}/\{1+\exp[(\phi-\phi_c)/\phi_m]\} + D_{0,conf}$, where $\phi_c = 0.32 \pm 0.02$, $\phi_v = 0.14 \pm 0.10$, $\phi_m = 0.0098 \pm 0.0068$, $D_{0,d} \approx 5.5 \times 10^{-12}$ m^2/s, and $D_{0,conf} = (1.9 \pm 0.9) \times 10^{-14}$ m^2/s ($R^2 = 0.778$).

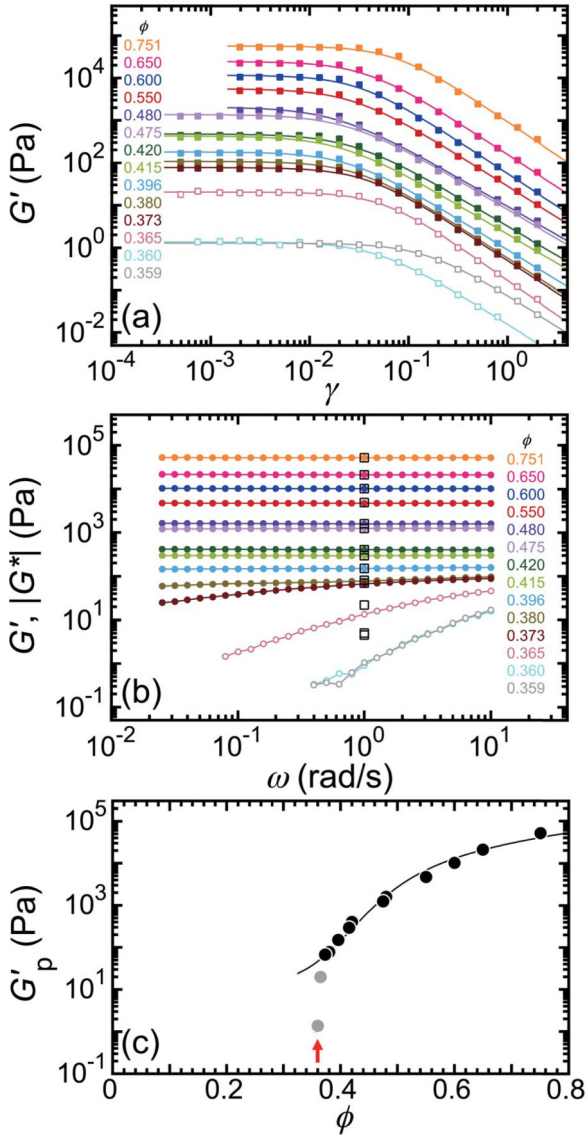

FIG. 3. Mechanical shear oscillatory measurements of elastic shear moduli. (a) Measured $G'(\gamma)$ at frequency $\omega = 1$ rad/s with fitting curves (see the text) for ϕ from 0.751 to 0.359 (top to bottom, color-code on left). (b) Measured $G'(\omega)$ at a fixed peak shear strain of $\gamma = 0.01$ for different ϕ and complex shear modulus $|G^*|(\omega)$ (open squares at $\omega = 1$ rad/s). (c) Plateau elastic shear modulus G'_p, obtained from strain sweeps in part (a), as a function of ϕ with the EEI model [38] prediction (solid line). Low-frequency relaxation of the system is evident at the frequency (i.e., 1 rad/s) associated with the strain sweeps at lower $\phi \leqslant 0.365$ (grayed markers). The red arrow highlights the lowest ϕ, where G'_p can be measured using mechanical rheometry.

the limited amount of data in the very dilute ϕ regime. The critical volume fraction ϕ_c for droplet unjamming, associated with the occurrence of the subdiffusive molecular motion, has been obtained from the fits of the $b_{\max}$-log-slope of effective MSDs, the D_0/D_1 ratio, and the low-b diffusion coefficient D_0, respectively, as functions of ϕ. The ϕ_c values inferred from all three of these approaches are highly consistent within the error range, having a standard deviation less than 2% of the average value (see the caption of Fig. 2 for fitting functions, parameters, and regression coefficients).

B. Mechanical shear rheometry

Mechanical shear oscillatory measurements are performed in both strain sweep and frequency sweep modes. The measured strain sweep data, $G'(\gamma)$, at a fixed frequency $\omega = 1$ rad/s, are fit to $G'(\gamma) = G'_p/[(\gamma/\gamma_y)^\kappa + 1]$, yielding the plateau shear modulus G'_p, the yield strain γ_y, and the high-strain power-law parameter κ that describes the decrease in the nonlinear G' beyond yielding [Fig. 3(a)]. For all ϕ in the range from 0.751 to 0.359, the elastic shear modulus G'_p at $\gamma = 0.01$ is in the low-strain plateau region. In the frequency sweeps, conducted at a peak shear strain $\gamma = 0.01$, the measured G' is frequency-independent over the range of ω from 10 to 0.02 rad/s for dense emulsion having $\phi \geqslant 0.380$ [Fig. 3(b)]. At such high ϕ, the measured plateau values of storage shear modulus G'_p are almost equal to the magnitude

of the complex shear modulus $G^*(\omega)$ at $\omega = 1$ rad/s over the frequency range explored. However, for $\phi \leqslant 0.373$, the frequency dependence of G' at $\gamma = 0.01$ renders the inaccuracy of determining G'_p from mechanical measurements using the $G'(\gamma)$ fits as in Fig. 3(a). For $\phi \geqslant 0.380$, the plateau shear elastic moduli G'_p are fit to the entropic, electrostatic, interfacial (EEI) model [38] using the following parameters: Droplet radius $a = 63$ nm, critical volume fraction for random close packing $\phi_{rcp} = 0.646$, Debye-screening length $\lambda_D = 4$ nm, surface tension $\sigma = 0.0098$ N/m, and surface potential $|\psi_0| = 52$ mV [Fig. 3(c)]. The loss of macroscopic elastic shear rigidity occurs very rapidly as ϕ is reduced in the range from 0.38 to 0.34.

C. Droplet MSDs from NMR and rheometry

The plateau MSDs associated with caged nanodroplet motion in the high-ϕ regime can be inferred from the mechanical rheometry measurements using the generalized Stokes-Einstein relation (GSER) of passive microrheology. We first deduce the three-dimensional (3D) droplet plateau MSDs, $\langle \Delta \boldsymbol{r}_d^2 \rangle_p$, from the measured G'_p at each ϕ by applying the GSER [15]: $\langle \Delta \boldsymbol{r}_d^2 \rangle_p = k_B T/(\pi a G'_p)$, where k_B is Boltzmann's constant, T is the temperature, and a is the average droplet radius. We then convert these 3D droplet plateau MSDs to 1D droplet plateau MSDs, $\langle \Delta z_d^2 \rangle_p$, by dividing by 3 since the disordered nanoemulsion is spatially isotropic. By contrast, in the lower-ϕ regime, near and below unjamming, we determine 1D total molecular MSDs assuming $\langle \Delta z^2 \rangle \approx 2D_0\Delta$ using the low-b diffusion coefficients from Fig. 2(c) for fixed $\Delta = 700$ ms. We hypothesize that these NMR-detected total molecular MSDs $\langle \Delta z^2 \rangle$ are associated with a superposition of the Brownian center-of-mass (COM) motion of the nanodroplets $\langle \Delta z_d^2 \rangle$, which varies with ϕ, and the confined molecular motion within the nanodroplets $\langle \Delta z_c^2 \rangle$, which is independent of ϕ. Assuming that the distributions for nanodroplet displacements and confined molecular motion in stationary nanodroplets are both Gaussian, we extract the 1D droplet MSDs $\langle \Delta z_d^2 \rangle$ for $\phi < 0.37$ through subtraction: $\langle \Delta z_d^2 \rangle = \langle \Delta z^2 \rangle - \langle \Delta z_c^2 \rangle$. To obtain a smooth match of the NMR-inferred droplet MSDs to the microrheologically inferred droplet MSDs, yielding smooth overlap at unjamming, we deduce a value of $\langle \Delta z_c^2 \rangle = 3.9 \times 10^{-14}$ m^2. This matching process yields a systematic 1D droplet MSD as a function of ϕ over the entire range of all measurements. This $\langle \Delta z_c^2 \rangle$ corresponds to a confined molecular diffusion coefficient of $D_{0,conf} = 2.8 \times 10^{-14}$ m^2 s^{-1}, which is slightly greater than but in reasonable accord (within one standard deviation) with the value $D_{0,conf} = (1.9 \pm 0.9) \times 10^{-14}$ m^2 s^{-1}, obtained from the fit of $D_0(\phi)$ at high ϕ in Fig. 2(c). If this alternative fit-parameter value were to be used instead, the agreement would still be quite reasonable overall, but the matching would not be quite as smooth near the droplet unjamming point. The droplet root-mean-square displacement, $\langle \Delta z_d^2 \rangle^{1/2}$, normalized by the effective interdroplet center-to-center spacing (i.e., which is approximately given by the droplet diameter $2a$), is reminiscent of the Lindemann ratio that has been used to quantify disorder-induced amorphization and to predict the melting point of crystalline materials [31,39] (see Fig. 4). In this presented disordered nanoemulsion system, we find that

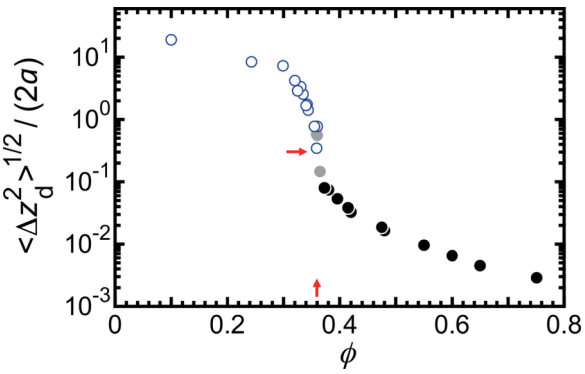

FIG. 4. Droplet root-mean-square displacement, $\langle \Delta z_d^2 \rangle^{1/2}$, normalized by the droplet diameter $2a$, as a function of ϕ. Solid black circles: plateau $\langle \Delta z_d^2 \rangle^{1/2}/(2a)$ deduced from the measured G'_p from Fig. 3(c) using the GSER; 3D MSDs from the GSER have been converted to 1D MSDs. Solid gray circles: the used small-strain G'_p in the GSER are extracted from fits of $G'(\gamma)$ for viscoelastic samples having small yield strain. Open blue circles: droplet $\langle \Delta z_d^2 \rangle^{1/2}/(2a)$ calculated for $\Delta = 700$ ms using NMR low-b diffusion coefficients D_0 for $\phi < 0.37$ from Fig. 2(c), where the total molecular probe 1D MSDs are $\langle \Delta z^2 \rangle = 2D_0\Delta$. To match droplet MSDs inferred from both sets of measurements at the unjamming point, we deduce that the confined molecular MSD $\langle \Delta z_c^2 \rangle$ is 3.9×10^{-14} m^2, and we subtract this value from $\langle \Delta z^2 \rangle$, yielding the droplet MSDs $\langle \Delta z_d^2 \rangle$. The horizontal red arrow indicates a Lindemann melting criterion of $\langle \Delta z_d^2 \rangle^{1/2}/(2a) = 0.3$, corresponding to a droplet unjamming (melting) point of $\phi_c \approx 0.36$.

the droplet unjamming point, determined via a Lindemann melting criterion of $\langle \Delta z_d^2 \rangle^{1/2}/(2a) = 0.3$, coincides with the value of $\phi_c \approx 0.36$ associated with the loss of zero-frequency plateau shear elasticity, determined using mechanical rheometry [see the arrows in Figs. 3(c) and 4]. Using alternative values for the Lindemann criterion, which are in the range 0.15–0.30 for most materials, does not substantially change this unjamming point.

IV. DISCUSSION AND CONCLUSION

These ^{19}F StE PFG-NMR measurements of concentrated nanoemulsions show that the attenuation, resulting from the total motion of ^{19}F-laden molecular probes diffusing within nanodroplets, changes dramatically when the nanodroplets unjam as ϕ is reduced and the low-frequency shear rigidity of the nanoemulsion vanishes. Thus, the total molecular motion reflects a superposition of center-of-mass motion of the nanodroplets as well as confined molecular diffusion of the ^{19}F-labeled silicone oil within the nanodroplets. At high ϕ, droplets are strongly jammed, and the nanoemulsion is a soft yet rigid solid; in this strongly jammed limit, the NMR attenuation decays resemble decays of liquids in other kinds of nanoporous solids. This indicates that the strongly jammed nanoemulsion can be considered as a closed-pore nanoporous solid having sufficiently large rigidity that only the highly confined molecular motion contributes substantially to the observed decay-to-plateau behavior. By contrast,

the superposition of the nanodroplet motion in combination with the confined molecular motion becomes evident through rapid changes in the NMR attenuation near and below the nanodroplet jamming point, where the nanoemulsion loses shear rigidity as ϕ is reduced. Moreover, the evidence of decay-to-plateau behavior at high-b disappears, and the decays become simple-exponential instead. In the dilute-ϕ limit, for the particular nanoemulsion that we have created and investigated, the NMR attenuation at low b is dominated by nanodroplet diffusion in the aqueous continuous phase, not by confined molecular motion of the oil within the nanodroplets. These new measurements and insights have been made possible through the fabrication of a custom-formulated size-fractionated O/W nanoemulsion that is composed of a perfluorinated copolymer silicone oil and a nonfluorinated surfactant.

By combining both NMR measurements with a passive microrheological interpretation of macroscopic mechanical rheometry measurements, we have obtained a master curve of droplet root-MSDs, normalized by the average diameter of the nanodroplets, as a function of ϕ both above and below the unjamming droplet volume fraction. This master curve enables us to show how droplet unjamming can be related to the classic idea of melting in terms of Lindemann's ratio. Using a Lindemann criterion of 0.3, known from other types of materials, we have shown that the ϕ associated with Lindemann melting coincides with ϕ_c associated with nanodroplet unjamming and the loss of low-frequency mechanical shear rigidity. The average diameter-normalized droplet MSDs as a function of ϕ for an emulsion system stabilized by screened electrostatic repulsion, in which the droplets are twice as large in radius as the droplets in our NMR study, have been reported in [40], showing the same ϕ-dependent trend as in Fig. 4 but with a higher droplet unjamming volume fraction due to the difference in droplet size. While we use the term "unjamming," we recognize that the screened-charge-stabilized system of nanodroplets may also be considered as a glassy colloidal system, below the electrostatic droplet-jamming point, that effectively undergoes a nonergodic to ergodic transition as ϕ is reduced; so, taken more broadly, the dramatic change we show also relates to the melting of disordered glassy systems, not just unjamming.

The model perfluorinated O/W nanoemulsion that we have designed, created, and studied using ^{19}F StE PFG-NMR is highly size-fractionated, has a disordered droplet structure, has short-range screened-charge repulsive interactions between the droplets, and effectively precludes interdroplet diffusion of perfluorinated oil molecules through the aqueous continuous phase. Therefore, the NMR attenuation in our measurements is not influenced by diffusion of probe molecules between nanodroplets. This enables us to interpret our NMR measurements more readily, as compared to prior studies in which oil molecules diffuse between droplets [30,41,42]. In addition, the high degree of size-fractionation of the nanodroplets enables us to fit the low-ϕ decays well using only a single exponential form.

Our investigations have revealed several key signatures in the PFG-NMR attenuation that are associated with unjamming and melting of a model soft colloidal solid; yet, many exciting directions still remain. For example, a higher magnetic field gradient could be used to explore the high-b regime to even larger b, potentially providing a direct measurement of the effective plateau of the NMR attenuation in the highly concentrated ϕ-regime. For instance, if more accurate and precise measurements can be made at higher b, it may be possible to deduce G'_p directly from the high-b plateau MSDs that can potentially be obtained. Fabricating and studying nanoemulsions that have a smaller average droplet radius would potentially be worthwhile, since this could further increase the sensitivity to nanodroplet motion in the jammed ϕ-regime relative to confined molecular motion. Thus, it would be interesting to perform similar studies on nanoemulsions having a range of different nanodroplet sizes. Moreover, varying the viscosity of the oil within the nanodroplets, through the molar mass of the oil, could also potentially enhance the NMR attenuation arising from nanodroplet motion relative to the confined molecular diffusion. Furthermore, our experiments broadly indicate that theories and simulations of the total motion of probe molecules within dense colloidal droplet probes would be interesting to explore through the glass and jamming transitions.

ACKNOWLEDGMENTS

Y.X. and M.L.N. contributed equally to this work. T.G.M. and J.D.S conceptualized the work; Y.X. and M.L.N. conducted the experiments. Y.X. and T.G.M. thank M. Pagenkopp for initial assistance with the design and fabrication of the perfluorinated O/W nanoemulsion, and the University of California–Los Angeles for financial support.

[1] T. Parella, Pulsed field gradients: A new tool for routine NMR, Magn. Reson. Chem. **36**, 467 (1998).

[2] F. Stallmach and P. Galvosas, Spin echo NMR diffusion studies, Annu. Rep. NMR Spectrosc. **61**, 51 (2007).

[3] M. Appel, G. Fleischer, J. Kärger, F. Fujara, and S. Siegel, NMR evidence of anomalous molecular diffusion due to structural confinement, Europhys. Lett. **34**, 483 (1996).

[4] A. Das, S. Jayanthi, H. S. M. V. Deepak, K. V. Ramanathan, A. Kumar, C. Dasgupta, and A. K. Sood, Single-file diffusion of confined water inside SWNTs: An NMR study, ACS Nano **4**, 1687 (2010).

[5] H. Wassenius, M. Nydén, and B. Vincent, NMR diffusion studies of translational properties of oil inside core–shell latex particles, J. Colloid Interface Sci. **264**, 538 (2003).

[6] O. Geier, R. Q. Snurr, F. Stallmach, and J. Kärger, Boundary effects of molecular diffusion in nanoporous materials: A pulsed field gradient nuclear magnetic resonance study, J. Chem. Phys. **120**, 367 (2004).

[7] S. Naumov, A. Khokhlov, R. Valiullin, J. Kärger, and P. A. Monson, Understanding capillary condensation and hysteresis in porous silicon: Network effects within independent pores, Phys. Rev. E **78**, 060601(R) (2008).

[8] R. L. Magin, Models of diffusion signal decay in magnetic resonance imaging: Capturing complexity, Concepts Magn. Reson. **45A**, e21401 (2016).

[9] A. I. Nakatani, M. D. Poliks, and E. T. Samulski, NMR investigation of chain deformation in sheared polymer fluids, Macromolecules **23**, 2686 (1990).

[10] P. T. Callaghan, Rheo-NMR: nuclear magnetic resonance and the rheology of complex fluids, Rep. Prog. Phys. **62**, 599 (1999).

[11] R. J. Cormier, C. Schmidt, and P. T. Callaghan, Director reorientation of a side-chain liquid crystalline polymer under extensional flow, J. Rheol. **48**, 881 (2004).

[12] N. H. Williamson, A. M. Dower, S. L. Codd, A. L. Broadbent, D. Gross, and J. D. Seymour, Glass Dynamics and Domain Size in a Solvent-Polymer Weak Gel Measured by Multidimensional Magnetic Resonance Relaxometry and Diffusometry, Phys. Rev. Lett. **122**, 068001 (2019).

[13] R. Kimmich and N. Fatkullin, Polymer chain dynamics and NMR, in *Advances in Polymer Science*, Vol. 170 (Springer, Berlin, 2004), pp. 1–113..

[14] P. T. Callaghan, Rheo-NMR and velocity imaging, Curr. Opin. Colloid Interface Sci. **11**, 13 (2006).

[15] T. G. Mason and D. A. Weitz, Optical Measurements of Frequency-Dependent Linear Viscoelastic Moduli of Complex Fluids, Phys. Rev. Lett. **74**, 1250 (1995).

[16] T. M. Squires and T. G. Mason, Fluid mechanics of microrheology, Annu. Rev. Fluid Mech. **42**, 413 (2010).

[17] T. G. Mason, Emulsiogenesis and the emergence of nanoemulsions, Matter **1**, 542 (2019).

[18] K. Meleson, S. Graves, and T. G. Mason, Formation of concentrated nanoemulsions by extreme shear, Soft Mater. **2**, 109 (2004).

[19] T. G. Mason, J. N. Wilking, K. Meleson, C. B. Chang, and S. M. Graves, Nanoemulsions: formation, structure, and physical properties, J. Phys.: Condens. Matter **18**, R635 (2006).

[20] A. Naseema, L. Kovooru, A. K. Behera, K. P. P. Kumar, and P. Srivastava, A critical review of synthesis procedures, applications and future potential of nanoemulsions, Adv. Colloid Interface Sci. **287**, 102318 (2021).

[21] H. S. Kim and T. G. Mason, Advances and challenges in the rheology of concentrated emulsions and nanoemulsions, Adv. Colloid Interface Sci. **247**, 397 (2017).

[22] T. Garasanin, T. Cosgrove, L. Marteaux, A. Kretschmer, A. Goodwin, and K. Zick, NMR self-diffusion studies on PDMS oil-in-water emulsion, Langmuir **18**, 10298 (2002).

[23] M. M. Fryd and T. G. Mason, Cerberus nanoemulsions produced by multidroplet flow-induced fusion, Langmuir **29**, 15787 (2013).

[24] K. J. Packer and C. Rees, Pulsed NMR studies of restricted diffusion. I. Droplet size distributions in emulsions, J. Colloid Interface Sci. **40**, 206 (1972).

[25] K. G. Hollingsworth and M. L. Johns, Measurement of emulsion droplet sizes using PFG NMR and regularization methods, J. Colloid Interface Sci. **258**, 383 (2003).

[26] A. A. Peña and G. J. Hirasaki, Enhanced characterization of oilfield emulsions via NMR diffusion and transverse relaxation experiments, Adv. Colloid Interface Sci. **105**, 103 (2003).

[27] P. T. Callaghan, *Translational Dynamics and Magnetic Resonance: Principles of Pulsed Gradient Spin Echo NMR* (Oxford University Press, Oxford, UK, 2011).

[28] C. Malmborg, D. Topgaard, and O. Söderman, NMR diffusometry and the short gradient pulse limit approximation, J. Magn. Reson. **169**, 85 (2004).

[29] R. Bernewitz, G. Guthausen, and H. P. Schuchmann, NMR on emulsions: characterisation of liquid dispersed systems, Magn. Reson. Chem. **49**, S93 (2011).

[30] P. T. Callaghan, A. Coy, T. P. J. Halpin, D. MacGowan, K. J. Packer, and F. O. Zelaya, Diffusion in porous systems and the influence of pore morphology in pulsed gradient spin-echo nuclear magnetic resonance studies, J. Chem. Phys. **97**, 651 (1992).

[31] V. Hoang, Melting of simple monatomic amorphous nanoparticles, J. Phys. Chem. C **116**, 14728 (2012).

[32] M. M. Fryd and T. G. Mason, Time-dependent nanoemulsion droplet size reduction by evaporative ripening, J. Phys. Chem. Lett. **1**, 3349 (2010).

[33] X. Zhu, M. M. Fryd, J.-R. Huang, and T. G. Mason, Optically probing nanoemulsion compositions, Phys. Chem. Chem. Phys. **14**, 2455 (2012).

[34] S. L. Codd and P. T. Callaghan, Spin echo analysis of restricted diffusion under generalized gradient waveforms: Planar, cylindrical, and spherical pores with wall relaxivity, J. Magn. Reson. **137**, 358 (1999).

[35] S. Meiboom and D. Gill, Modified spin-echo method for measuring nuclear relaxation times, Rev. Sci. Instrum. **29**, 688 (1958).

[36] T. G. Mason, H. Gang, and D. A. Weitz, Diffusing-wave-spectroscopy measurements of viscoelasticity of complex fluids, J. Opt. Soc. Am. A **14**, 139 (1997).

[37] M. Khan and T. G. Mason, Local collective motion analysis for multi-probe dynamic imaging and microrheology, J. Phys.: Condens. Matter **28**, 305201 (2016).

[38] H. S. Kim, F. Scheffold, and T. G. Mason, Entropic, electrostatic, and interfacial regimes in concentrated disordered ionic emulsions, Rheol. Acta **55**, 683 (2016).

[39] N. Q. Lam, P. R. Okamoto, and M. Li, Disorder-induced amorphization, J. Nucl. Mater. **251**, 89 (1997).

[40] M. Braibanti, H. S. Kim, N. Şenbil, M. J. Pagenkopp, T. G. Mason, and F. Scheffold, The liquid-glass-jamming transition in disordered ionic nanoemulsions, Sci. Rep. **7**, 13879 (2017).

[41] J. Pfeuffer, U. Flögel, W. Dreher, and D. Leibfritz, Restricted diffusion and exchange of intracellular water: theoretical modelling and diffusion time dependence of ^{1}H NMR measurements on perfused glial cells, NMR Biomed. **11**, 19 (1998).

[42] L. Vermeir, P. Sabatino, M. Balcaen, A. Declerck, K. Dewettinck, J. C. Martins, and P. Van der Meeren, Effect of molecular exchange on water droplet size analysis in W/O emulsions as determined by diffusion NMR, J. Colloid Interface Sci. **463**, 128 (2016).